

6A Optics Contamination

*Charles Tarrío, Shannon B. Hill, Robert F. Berg,
(National Institute of Standards and Technology)*

and

Saša Bajt (Deutsches Elektronen-Synchrotron)

6A.1 Introduction

The performance of extreme ultraviolet (EUV) scanners in the field testifies that formidable obstacles to high-volume EUVL manufacturing have been overcome. A key element in this progress has been the virtual elimination of optics contamination as a major hurdle, a development involving several efforts worldwide and stretching over more than a decade. We will describe the chemical processes that lead to contamination, some of the research efforts directed at understanding them, and the resulting mitigation techniques that were developed.

Ionizing radiation creates chemical reactions that contaminate optical surfaces in an atmosphere with even trace amounts of water vapor or organic molecules. Organic molecules adsorbed on the optical surface can be cracked by both the energetic radiation and the secondary electrons it produces, creating a contaminating carbon film. Adsorbed water molecules can be activated to generate strong oxidizers that attack the optical surface itself. However, these two processes can counteract each other, and in the presence of a significant partial pressure of organic molecules or a carbon overlayer, the oxidation by radicals from the water vapor can be reduced or the carbon overlayer can be etched.

The problems of carbonization and oxidation of optics by ionizing radiation had been observed much earlier in satellite instruments exposed to UV radiation from the sun and in experiments at synchrotron facilities. EUVL was particularly sensitive to this issue due to the expense of EUV photon production and the many optic surfaces between the source and wafer. Even a 1 % loss on each optic would reduce the total transmission below the threshold of economic viability. The problem was compounded by the fact that the optics, which consist of precisely figured, ultra-smooth, mirrors coated by 40 or more molybdenum/silicon bilayers, could be irreversibly damaged by oxidation or many carbon removal methods.

The elimination of optics contamination benefitted from experience gathered in the pre-production tools. The first major advance came from the development of an oxidation-resistant cap layer that protected the underlying, less oxygen-resistant, molybdenum and silicon. The next advance was dealing with the carbonization caused by the unavoidable organics coming from resist outgassing and some parts of the unbaked vacuum system. Cleaning of that carbonization by atomic hydrogen was shown to work without damaging the optics.¹ In 2006, ASML directed the development of a resist outgas test. The goal was to eliminate resists that were too carbonizing and thus would require too frequent cleaning of the projection optics and those resists that had elements that were thought to be not cleanable with atomic hydrogen (e.g., F, Cl, I, Br, P, and S). However, over the next seven years, users of the scanners in the field found that the carbon deposition rates were low enough that they could be managed without significant reduction in productivity for all reasonable chemically amplified resists. The present scanners operate in an atmosphere of low pressure hydrogen, and the interaction of EUV and hydrogen gas produces hydrogen radicals², which significantly reduces carbon deposition rate. In addition, the scanners have well designed dynamic gas curtains³ that act to reduce the amount of resist outgassing that impinges on the optics. The only remaining concern is that one or more of the elements used in the newer metal-containing resists might produce contamination that cannot be

cleaned by hydrogen radicals. Since development of novel resists is largely in the proprietary phase, we will not discuss that source of contamination here.

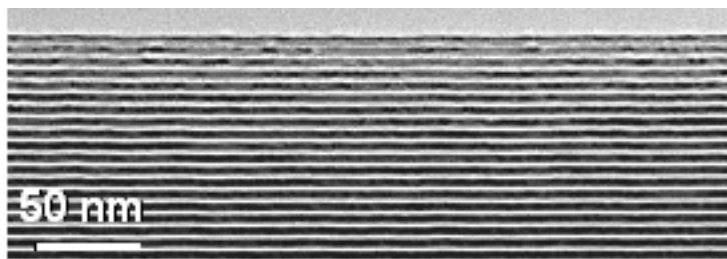


Figure 1 Cross-section transmission electron microscopy (TEM) image of the top part of a typical EUV multilayer. The multilayer mirror usually consists of 40 Mo/Si pairs. Silicon (low Z) is less absorbing and shown here as bright layers, while Mo (high Z) layers are dark.

6A.1.2 Background

The problem of contamination resulting from ionizing radiation has long been known. Berthelot and Gaudenchon first observed the polymerization of organic molecules under ultraviolet illumination in 1910.⁴ Contaminating films cause widespread problems in electron microscopy, including both charging of electron optics⁵ and changes in specimens after long-term illumination.⁶ Hillier⁷ reviewed existing evidence in 1948 and correctly noted that the growth is due to electron-beam-induced deposition of carbon from organic molecules present in the vacuum system.

In 1983, Boller et al.⁸ investigated the carbon contamination associated with synchrotron radiation. In his model the interaction between energetic photons and a mirror surface creates secondary electrons that have sufficient energy to break the bonds of adsorbed organic molecules, eventually forming a solid carbonaceous layer or bonding with the surface of the mirror. The growth of carbon often led to an unacceptable decrease in reflectivity and a need to clean the carbon from the mirror.

The problem was known also to astrophysicists using spacecraft to observe the sun. The first long-term observation of this effect was on the Solar and Heliospheric Observatory (SOHO, ref. 9), which was launched in 1995. SOHO instruments exhibited various degrees of degradation, summarized in ref. 10. The environment of SOHO has some similarity with that of an EUVL tool in that water and organics outgassed from the spacecraft can interact with the solar EUV. However, the gas pressures are lower and the incident spectrum is considerably different: the solar spectrum is broader, the intensity is lower, and the radiation is continuous-wave rather than delivered in ns-duration pulses.

We shall focus on the EUVL projection optics, which are near-normal-incidence mirrors consisting of precisely figured substrates coated with alternating layers of Mo and Si (see **Fig. 1**). Such multilayer (ML) coatings, first developed by Spiller¹¹, enable high reflectivity and wavelength selectivity of EUV mirrors. In addition to the contamination problems observed on all optics exposed to ionizing radiation, there was an initial concern about the stability of the multilayers against interdiffusion. An early study reported that Mo/Si multi-layer mirrors (MLMs) have long-term stability at room temperature.¹² In this study, a MoSi mirror with a 1 nm C capping layer was

measured, stored in air for 20 months, and remeasured, with no observable decrease in the reflectivity. On the other hand, Mo-terminated multilayers were shown to degrade to about 75 % of their original reflectivity when stored in air due to oxidation of the Mo top layer.¹³ In a study of radiation hardness against interdiffusion, a Mo/Si multilayer was exposed to monochromatic undulator radiation and found not to degrade.¹⁴ The exposed dose to the mirrors was equivalent to a 1.2-year EUV exposure in the low-throughput lithography system considered at that time. The predicted optics lifetime was based on a nine-hour exposure with an average intensity of 0.75 W/cm² and vacuum pressure less than 5×10⁻⁸ mbar (1 mbar=100 Pa). These results thus overestimated the optics lifetime because they were performed in high vacuum and not in a realistic environment typical of an EUV exposure tool, with remnants of water vapor and other contaminants. Other lifetime studies performed on Si-capped MLMs exposed the optics to EUV radiation doses equivalent to several months of lithographic conditions (assuming a higher than 10 wafers/hr throughput).¹⁵ It was observed that the surface carbon deposition was dependent on the residual gas concentration in the vacuum chamber. However, no structural damage was observed within the bulk of the MLMs. In addition, the reflectivity was fully recovered with ozone cleaning, although ozone overexposure can lead to damage via surface-layer oxidation.

6A.1.3 The chemical processes

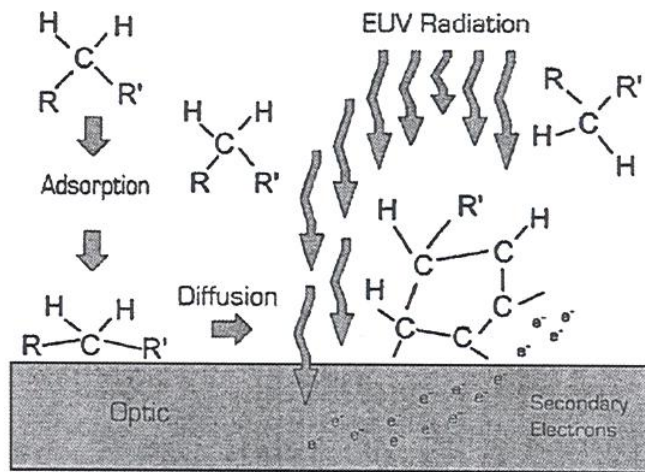


Figure 2: Simple model showing the main radiation-induced processes related to carbon contamination. [from ref. 16.]

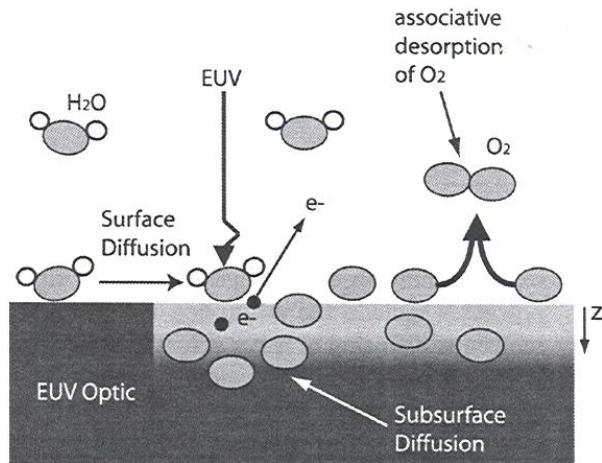


Figure 3: Simple model showing the radiation-induced processes leading to oxidation of the optics surface. [From ref. 17]

Figures 2 and 3 show schematically the processes that lead to carbonization and oxidation. Several pathways are available after molecules adsorb onto the surface. They may diffuse along the surface or thermally desorb. A photon may directly break a bond or stimulate desorption of the molecule, or it may do either of these indirectly via secondary-electron emission from the mirror. If an organic molecule is fragmented, this will lead to carbon deposition on the surface. If a water molecule is fragmented, the oxygen may diffuse into the mirror surface and create or increase the oxide layer.

6A.2. Optics contamination research

6A.2.1 Carbonization and Oxidation; Photons or Photoelectrons

In high volume manufacturing, the repeated introduction and EUV exposure of photoresist-coated wafers in the scanner means that the scanner's atmosphere will always contain levels of water and organics that are higher than in a research tool. The resulting combination of oxidation and carbonization will depend on the balance between the two species and their activation by the EUV. The literature, however, is not clear as to whether the activation is predominantly done by the EUV itself or by the secondary electrons generated by the EUV.

Boller et al.⁸ carried out measurements of carbon growth using an undispersed synchrotron beam at different background pressures, doses, and temperatures. They constructed a semi-quantitative model based on incident molecular flux, cracking, and desorption. They observed a rapid growth of carbon for the first 5 nm, then a less rapid growth. A similar pattern was observed in the secondary-electron yield, which was consistent with the smaller electron yield of carbon, leading to their model of secondary electrons as the predominant agent. The growth rate was weakly dependent on pressure because the pressure was governed only by a pumpdown time, so that the pressure of water vapor, a mitigating gas, was considerably higher than any hydrocarbons. They observed a much higher growth at room temperature than at elevated temperatures, which is expected due to the lower adsorbate coverage at higher temperatures.

Hillier⁷ investigated carbon growth in an electron microscope. He found that growth was very slow when the beam was illuminating only the thin-film sample being investigated, but much faster if part of the beam was hitting the support grid. This also seems to indicate the mechanism is initiated by secondary electrons.

Hollenshead and Klebanoff,^{16,17} on the other hand, found via a combination of simulations and experiments that photoabsorption in the adsorbate is the primary mechanism driving carbon growth and oxidation. They calculated similar cross-sections for photons and secondary electrons, and since the measured total electron yield was just a few percent, they concluded that the vast majority of damage was due to photons. Their models also predicted reduced contamination at higher temperatures.

Leontowich and Hitchcock^{18,19} bear out the work of Boller et al.⁸ They used an EUV microscope to focus the radiation down into a tunable monochromatic beam which irradiated a surface in an atmosphere of organic contaminants. They found that the rate of carbon growth varied strongly with the photon absorption cross section of the deposited carbon and not with that of the precursor molecules. With the reasonable assumption that the secondary electron emission of the deposited carbon varied with the carbon cross section, one can conclude that the secondary emission is much more effective in cracking the organic species than the impinging photon flux. This is the most direct evidence that the primary growth mechanism is due to secondary electrons.

6.A.2.2 The elimination of oxidation as a problem; requirements for oxidation-resistant cap layers

The EUVL community recognized the need for an oxidation-resistant cap layer.²⁰ Early experience with Si-capped Mo/Si MLMs revealed that the Si was not very resistant to EUV-induced oxidation. (Mo oxidizes more readily than Si and was never used as a terminal or cap layer.)

An ideal capping layer must satisfy many requirements, starting with its optical properties.²¹ The reflectivity loss of the mirror at 13.5 nm due to absorption by the capping layer should be minimized. Initial screening of various materials can be done using appropriate software and optical constants data,^{22,23} but given the need to maintain the highest possible reflectivity, one must actually test each of the initial candidate materials to eliminate any uncertainties.

The structure of the capping layer is also important. It must be smooth (of order 0.1 nm RMS high spatial frequency roughness) and continuous, even though the layer is only 1 to 3 nm thick. These characteristics apply not only to the surface, but also to the interaction of the cap layer with the underlying layer of Mo or Si. Deposition must be done at temperatures below 100 °C to avoid intermixing in the underlying MLM stack, and it must generate minimal stresses in the film stack. The nanostructure of the capping layer, which plays a crucial role in surface chemistry, needs to be well-known and controllable. The capping layer should be impermeable to carbon and oxygen diffusion, either into or out of the MLM. If the capping layer is polycrystalline, this might require a specific crystallographic texture. Likewise, if the capping layer is amorphous, it should have no mobile vacancies.

Surface chemistry must also be considered. The capping layer materials must be chemically inert with respect to air, the background gases (H_2 , H_2O , CO , CO_2 , hydrocarbons), and the stack materials. Different materials will also respond in different ways to mitigation and removal methods. Unfortunately, most of the existing surface science data are derived from well-characterized single-crystal sample surfaces. In practice, the capping layers are amorphous or polycrystalline, likely with high concentrations of defects and vacancies, so properties based on ideal single-crystal surfaces might be quite different from the properties of realistic capping layer surfaces.

Capping layer materials must be thermally stable and stable against EUV radiation-induced processes. Finally, the capping layer should be cost-effective and in accordance with environmental, health, and safety regulations during its manufacture and use.

6.A.2.3 Development of contamination resistant cap layers

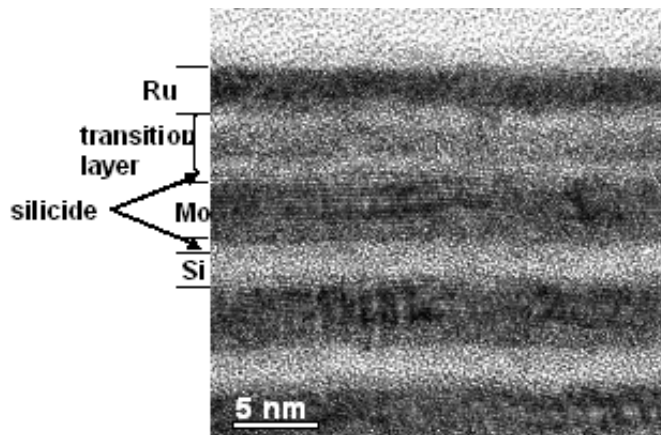


Figure 4: Cross section TEM image of an EUV multilayer showing the microstructure of the surface layers. The top dark layer is polycrystalline Ru deposited on the top of transition layer. Polycrystalline molybdenum and amorphous silicon layers are separated by thin, amorphous silicide layers.

Because of the proprietary nature of some of the materials being tested as capping layers, most of this section will be limited to the development of ruthenium capping layers, which were chosen by SEMATECH as a standard benchmark capping layer and where the results have been made public.

Figure 4 shows a cross-section of the surface region of a Ru-capped MLM. Ru capping layers prepared with variations of voltage, current, sputtering gas, and target material were tested for their oxidation and thermal stability. The best capping layer was prepared using Ar sputtering gas and a metallic Ru target. TEM analysis of its microstructure²⁴ showed that it was the only one with preferentially oriented grains. In particular the Ru was polycrystalline with an average grain size of about 3.5 nm and a preferential growth orientation with Ru(0001) crystal planes parallel to the specimen surface. Based on limited TEM data it appears that the Ru capping layers of other preparations had smaller, randomly oriented, and mostly oxidized grains.

As part of a SEMATECH funded project, Lawrence Livermore National Laboratory (LLNL) also fabricated and tested five more capping layer candidates. In descending order of reflectivity, measured as well as calculated, the candidate materials were SiC, yttria stabilized zirconia, MoSi₂, PdAu, and Pd.²⁵ Due to limited funding the capping layer deposition processes were not optimized and the capping layers had different deficiencies. For example, the Pd and PdAu capping layers showed island growth, and were detected in the layers below the capping layer, which could possibly have been mitigated with a diffusion-boundary layer. The other materials appeared to allow oxidation of a few lower layers. None of these materials outperformed Ru.

After Ru, the most widely used capping layer is TiO₂, which has favorable optical and surface reactivity properties. Adding a 2 nm thick TiO₂ capping layer reduces the reflectivity by only 0.8%. This material belongs to the class of semiconductors with a relatively wide band gap in the near UV. Exposing TiO₂ to photons with energy greater than the band gap produces charge carriers, which causes oxidation-reduction reactions to occur on the TiO₂ surface. A TiO₂ thin film has strong oxidizing power and high photocatalytic activity for hydrocarbon oxidation²⁶, which suggests that a TiO₂ capping layer could be self-cleaning. Work by Kim et al.²⁷ indicates that reactive magnetron sputtering allows control of the structure, composition and properties of TiO₂ films. Studies at LLNL found that reactive radio-frequency (RF) sputtering of a TiO₂ target with Ar:O₂ sputtering gas produced a TiO₂ capping layer with good properties: The MLM had a reflectivity that was greater than 66 %, and its lifetime under exposure to H₂O vapor was longer than for a Ru-capped MLM²⁸ TEM studies showed that the TiO₂ capping layer was amorphous, but it was continuous and fully covered the multilayer. Furthermore, the TiO₂ layer formed a sharp interface with Si so that no diffusion barrier was necessary. However, XPS and STEM analysis indicated that Ar gas was incorporated into the TiO₂ capping layer. Yulin et al.²⁹ optimized deposition processes for MoSi multilayers with TiO₂ and RuO₂ cap layers, both with engineered interfaces.

Work on other alternative cap layers, many of which were discussed theoretically in ref. 20, continues. Kriese³⁰ recently investigated SiO₂ and ZrO₂ as potential cap layers. Unfortunately, the lack of a fundamental understanding of the surface chemistry in realistic environments makes it difficult to optimize the capping layer. For the present, ruthenium appears to be adequately resistant to damage caused by oxidation and hydrogen cleaning.

Industry eventually made the development of capping layers confidential, in part because the environmental conditions in the scanner (residual gas pressures and species) were confidential. Also, while depositing Ru can be done in DC mode, depositing oxides can require RF mode or pulsed laser deposition, elevated temperatures, and a sputter gas mixture of inert gas and oxygen, methods which are more complicated and riskier. This was the primary reason for SEMATECH's decision to use Ru as a standard benchmark capping layer for optics lifetime tests.

6A.3. Optics contamination experiments

6A.3.1. Facilities

The majority of early optics lifetime tests were performed both with electron (see **Fig. 5**) and synchrotron EUV beams (see **Fig. 6**) in specially built test chambers. The contamination test chambers, which could accommodate high gas pressures (up to 10^{-2} mbar), were typically separated from the upstream components through differential pumping or by a thin-film filter. The use of electron-beam irradiation was justified by initial evidence that irradiation with keV-energy electrons and 13.5 nm EUV photons resulted in similar oxidation rates on Si-capped MLs, with 1 μ A of electron-beam current roughly equivalent to 1 mW of EUV power.³¹ However, the apparent equivalence of the two methods was short-lived: results on Ru-capped MLs³² showed differences due to the different surface chemistry and damage mechanisms.

In recent years most lifetime testing has been done with EUV photons. After initial work^{30,32} at LBNL's Advanced Light Source (ALS), most of the testing of optics lifetimes proceeded on dedicated EUV sources. The Japanese efforts are centered at BL-3 beamline in the New-SUBARU synchrotron facility.³³ The research guided by ASML is performed at several locations: At the ASML and the TNO laboratories with Hollow Cathode Triggered (HCT) pulsed sources;³⁴ and at the PTB Radiometry Laboratory, BESSY II, in Germany,³⁵ initially on the U180 undulator beamline³⁶ and later on the DLW 20 dipole bending magnet beamline.³⁷ Work in the U.S. has centered at two beamlines (BL1b and BL8) at the NIST Synchrotron Ultraviolet Radiation Facility (SURF III).^{38,39} Comparison of results among the different facilities requires careful consideration of the exposure bandwidth, intensity, and time structure (i.e., pulsed duty factor and peak vs. average intensity), the temperature, and the vacuum environment, including the calibration of partial pressure measurements.

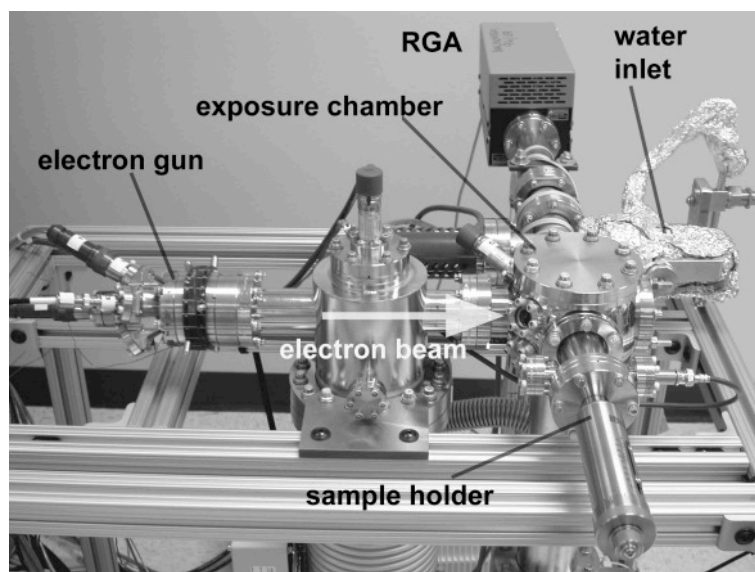


Figure 5 Initial lifetime experiments were performed with electron beams. This photograph shows a setup at Sandia National Laboratory (SNL).

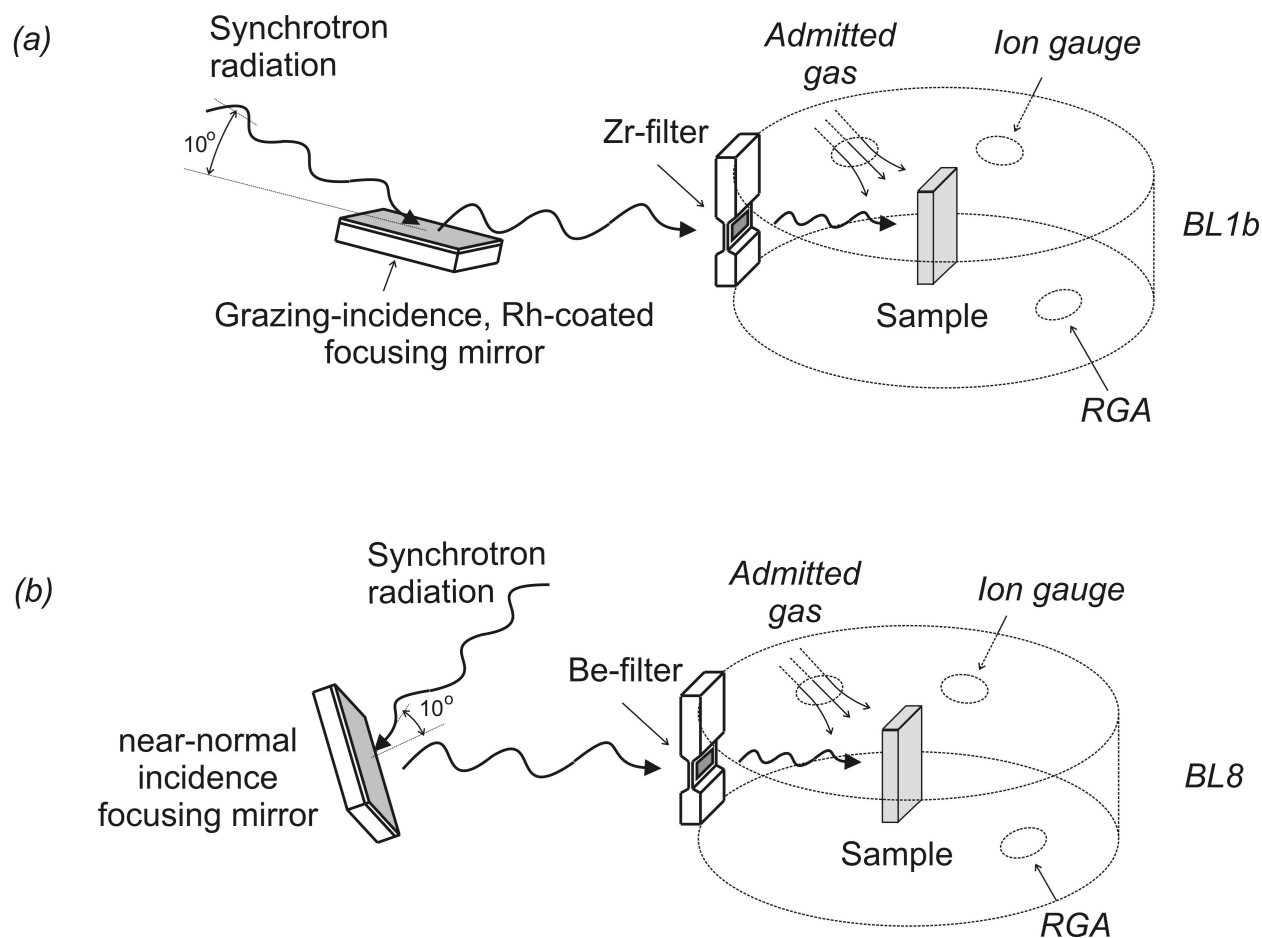


Figure 6. Schematics of the end-stations on (a) beamline 1b (BL1b) and (b) beamline 8 (BL8) at the NIST Synchrotron Ultraviolet Radiation Facility used for EUV-optics lifetime studies. Both have residual gas analyzers (RGA) to monitor the cleanliness and composition of the vacuum.

6A.3.2 Carbonization: admitted-gas studies

Although the initial contamination tests focused on the oxidation resistance of MLMs, lifetime testing performed under “real” tool conditions showed that ambient hydrocarbons play an important role in reducing oxidation in Ru capping layers.⁴⁰ In accelerated experiments where water vapor pressures were high ($>5 \times 10^{-7}$ mbar), the EUV-induced damage on Ru capped MLMs decreased with increasing levels of water.⁴¹ These results were explained by the presence of low-mass carbon-containing species in the chamber,^{41,42} as follows. A residual gas analysis made prior to the admission of the water showed low levels of low-mass carbon species. Subsequent measurements also could not detect these species coming from the water source. Hence, most likely they were displaced from the vacuum-chamber walls by the admitted water vapor.

These early observations coupled with the observation of the carbonization of optics and masks in the early test tools led to more extensive admitted-gas tests with organic molecules. These experiments were carried out in the facilities described in section 6A.3.2.1. Admitted gases have

been selected to include resist outgas products⁴³ and other molecules observed in scanners,⁴⁴ and covering a wide range of vapor pressures. In order to make an informed guess as to the contamination rates from atmospheres containing organics, both the contaminant partial pressure and EUV intensity had to be varied over significant ranges.

6A.3.2.1. Intensity dependence

Intensity dependence falls between two limiting regimes: the low intensity region in which the carbon growth rate depends linearly on intensity and on the coverage isotherm of the contaminating species; and the high intensity or intensity saturated region where the carbon growth rate depends only on the impingement rate of the contaminant molecule. In addition, one must also consider the temporal characteristics of the source. Synchrotron sources used at some of the testing facilities which have pulse repetition rates in the MHz or tens of MHz range can be considered quasi-cw. The pulsed sources used other experimental facilities have pulsed source with repetition rates between 0.1 kHz and 10 kHz. One expects that most pulsed sources used in these facilities have relatively small duty factors so that at an average intensity that would be considered to be in the low intensity region for a cw or quasi-cw source, the instantaneous intensity in the pulse is actually in the intensity saturated regime where the amount of contamination per photon is less than in the linear regime. Thus for a given partial pressure of a contaminant species, we would expect less contamination per unit dose for a pulsed source operating at the same average intensity as a cw source, a difference that has actually been observed by Wolschrijn, et al.⁴⁵

Exposing a sample at several pressures, each at several EUV intensities would be time consuming. To avoid this issue, Hill et al.⁴⁶ took advantage of the inherently quasi-Gaussian intensity distribution of their synchrotron beam at NIST, which could be accurately characterized with high spatial resolution. Thickness maps of the resulting carbon spots were then measured using both XPS and spectroscopic ellipsometry with sufficient spatial resolution that each map location could be correlated with a known EUV intensity. With this technique the intensity dependence at a given pressure could be measured over a wide range of intensities with a single exposure.

Figure 7 shows the results of such measurements using the high-intensity, broadband-EUV exposure facility on BL1b at NIST.⁴⁷ In order to eliminate effects due to standing-wave resonances in MLMs, these and subsequent measurements were made with trilayer samples consisting of the final three layers of a multilayer. The contamination rate scales linearly with intensity for highly contaminating species like toluene, tetradecane and diethylbenzene at partial pressures above 1×10^{-7} mbar. At lower pressures, however, the contamination rate begins to saturate with increasing intensity for these species, while benzene shows signs of saturation even at the elevated pressures. This behavior is consistent with two regimes of carbon growth for intensities significantly above or below a certain threshold or saturation intensity, I_{sat} . For intensities below I_{sat} , the rate at which adsorbed gas molecules are converted to deposited C is much smaller than the rate of thermal desorption. Hence, the C growth rate is proportional to the coverage of adsorbed precursor molecules on the surface in equilibrium with the ambient partial pressure. Since this steady-state coverage is not significantly affected by the EUV-induced cracking, the contamination rate scales linearly with intensity. For intensities much above I_{sat} , the situation is reversed; every molecule that adsorbs on the surface is likely to undergo a photon-stimulated reaction and adds to

the growing carbon layer before it thermally desorbs. In this regime the contamination rate will be independent of intensity and proportional to the rate at which molecules arrive at the surface, i.e., proportional to pressure.

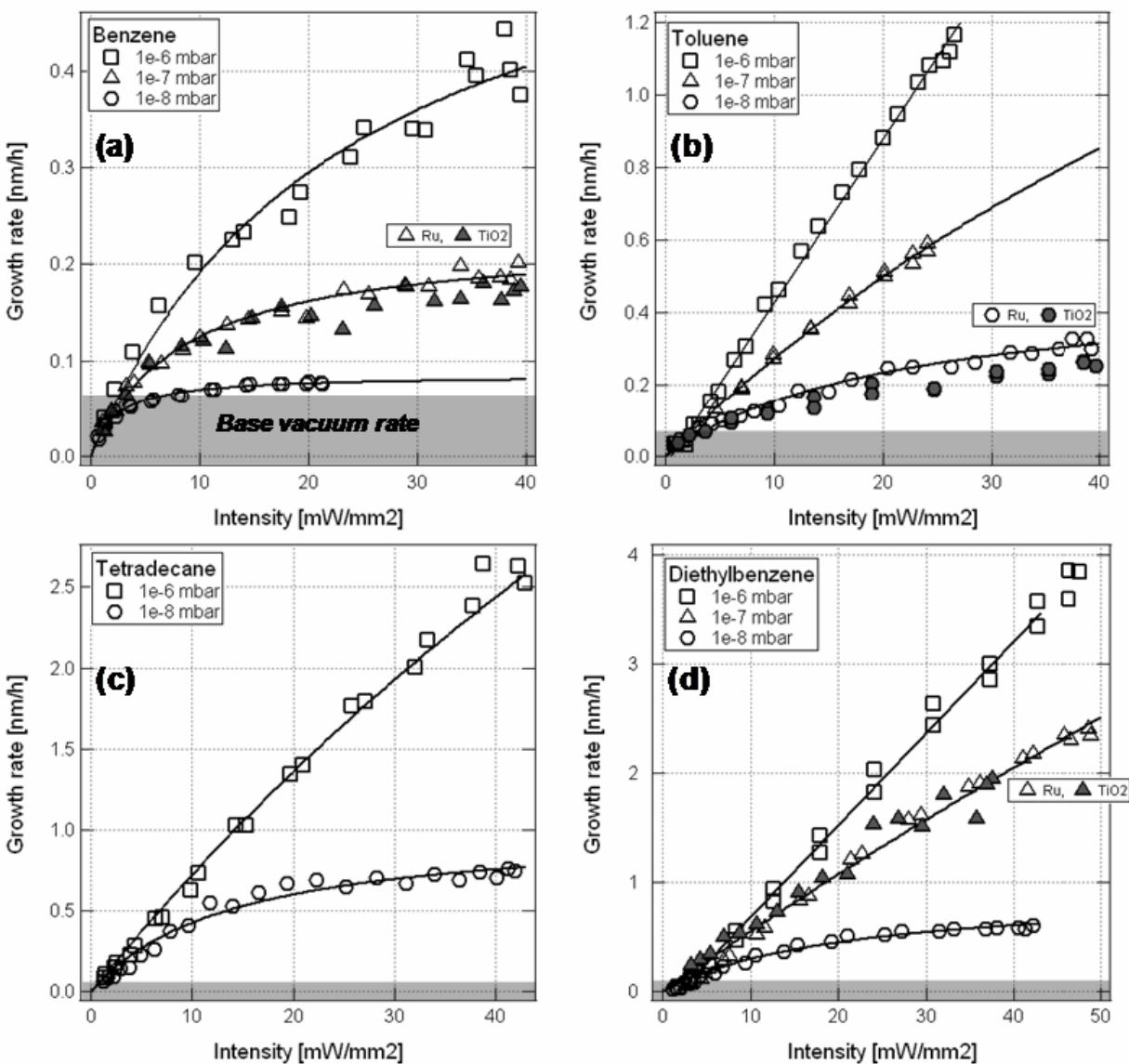


Figure 7. Contamination rates for Ru-capped (open symbols) and TiO₂-capped (shaded symbols) multilayer samples exposed to broadband-EUV on BL1b at the NIST synchrotron over a range of partial pressures of (a) benzene, (b) toluene, (c) tetradecane, and (d) diethylbenzene. The rates are determined by dividing the XPS-measured thickness by the exposure time. Partial pressures are reported without correction for ionization gauge sensitivity factors. Grey bands represent the intensity-independent background contamination rate of ≈ 0.07 nm/h with no admitted gas.

6A.3.2.2 Pressure dependence

The linear pressure scaling in the mass-limited regime is indicated by the data in **Fig. 7(a)**. After subtraction of the background contamination rate (indicated by the gray band), the asymptotic mass-limited rates for $I \gg I_{sat}$ increases by roughly an order of magnitude for each decade of pressure rise from 10^{-8} to 10^{-6} mbar.

For intensities below I_{sat} , in the photon-limited regime, the time-rate of carbon growth (nanometers per hour) scales linearly with intensity, and the deposition is best characterized by the dose-rate of carbon growth [$\text{nm}/(\text{mJ}/\text{mm}^2)$] which is given by the constant slope of the linear portions of the plots in **Fig. 7**, for $I \ll I_{sat}$. It is clear from casual inspection that the slopes of the lines for 10^{-6} mbar curves in **Fig. 7** (b and d) are not 10 times larger than those for the 10^{-7} mbar data. This suggests that the pressure scaling of the dose-rate of carbon growth in the photon-limited regime is highly sublinear. Indeed, a more extensive set of exposures on the lower-intensity, narrow-band BL8 at NIST found the quasi-logarithmic dependence on pressure shown in **Fig. 8** for several species. Here the dose-rate of C growth has been converted to a time-rate of growth by reporting values at a specific intensity of $1 \text{ mW}/\text{mm}^2$.

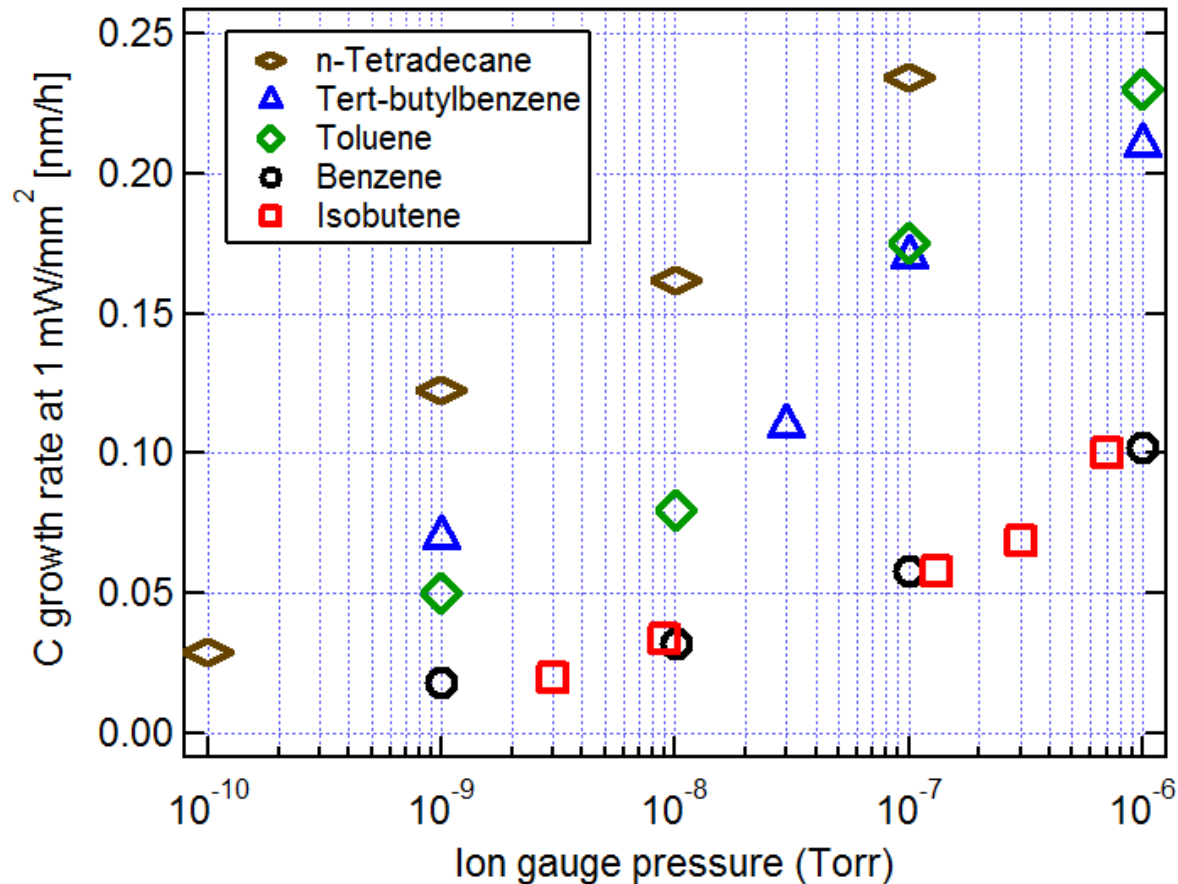


Figure 8. Carbon growth rate on TiO_2 -capped trilayer samples exposed to $1 \text{ mW}/\text{mm}^2$ 13.5 nm radiation on BL8 of the NIST synchrotron in the presence of various pressures of five contaminant gases. Absolute partial pressures are accurate to within a factor of ± 3 due to uncertainties in ionization gauge sensitivity and calibration for each gas. Relative uncertainties between pressures of a given gas are $\pm 20\%$. Molecules are: n-tetradecane, $\text{C}_{14}\text{H}_{30}$; tert-butylbenzene, $\text{C}_{10}\text{H}_{14}$; toluene, C_7H_8 ; benzene, C_6H_6 , and isobutene, C_4H_8 .

The highly sub-linear pressure dependence can be understood by considering that the surface density (coverage) of adsorbed molecules in the absence of EUV irradiation is determined by the equilibrium established between the impingement rate (and sticking coefficient) of molecules on the surface and the rate at which they are thermally desorbed. Direct measurements of equilibrium coverages by Yakshinskiy et al. have demonstrated that the desorption rate increases with increasing coverage.^{48,49} This results in the observed sub-linear, quasi-logarithmic pressure scaling of equilibrium coverage, and hence contamination rates, because the linear increase of impingement rate with pressure must compete with a simultaneous increase in desorption rate as the coverage rises with pressure. One possible reason for the coverage-dependent thermal desorption rate is that surface defects lead to a distribution of adsorption sites and energies. This model is often referred to as a Temkin-like isotherm,⁵⁰ as opposed to the more commonly assumed Langmuir isotherm,⁵¹ which assumes a constant, uniform adsorption energy.

The fact that carbon growth rates in the photon-limited regime seem to have a strongly sub-linear dependence on pressure over many decades creates difficulties in extrapolating the results of some admitted gas tests to extremely low pressures. As illustrated in **Figure 9**, if a single point is measured in a high-growth region and linearly extrapolated to zero pressure, the lowest curve is obtained. A Langmuir extrapolation using the top three points gives something intermediate, while using all the points and assuming a power-law dependence gives a result four orders of magnitude higher than the linear extrapolation. If, however, the intensity is high enough that the contamination will occur entirely in the mass-limited regime for both the measurements and the projected operating conditions, it is reasonable to extrapolate using a linear pressure dependence.

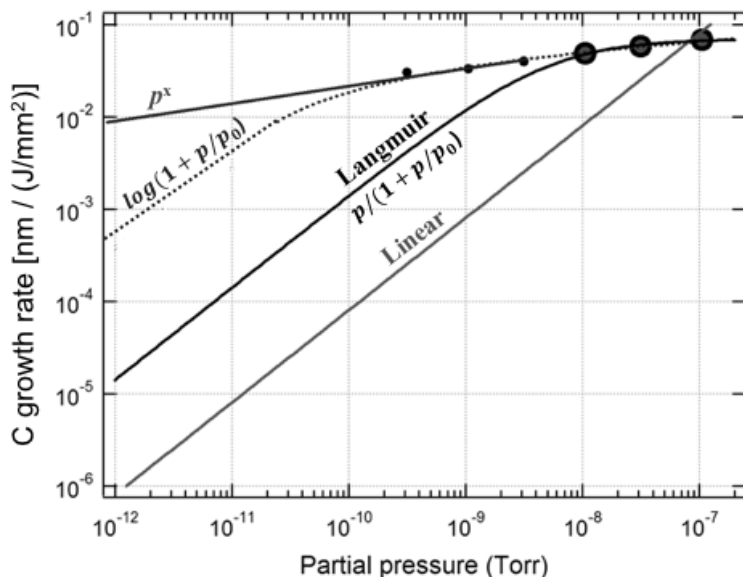


Figure 9. Dose-rate of contamination growth as a function of the partial pressure of tert-butylbenzene, with four potential extrapolations of measured data to very low pressures.

The carbon growth rate obviously depends also on the type of molecule. The heavier organics have more carbon atoms, and they also in general are stickier, so one would assume that the contamination rate would increase, possibly faster than linearly, with mass. However, the growth

rates for a given pressure have a more complicated dependence on mass. As shown in **fig. 8**, the growth rate from toluene, with seven carbons, is almost twice that of benzene with six carbons, while that of isobutene, with four carbons is roughly equal to that of benzene.⁵² The vapor pressure of isobutene is also much higher than that of benzene, so the coverage would seem to be much lower, again leading to less carbon growth.

6A.3.2.3. Wavelength dependence

The carbon growth rates were measured for three different species under identical conditions when irradiated by different bandwidths of EUV/UV. Three different filters were used on BL8 at NIST to achieve the different irradiance spectra shown in **Fig. 10 (b)**. Also included is the broad-band output of BL1b. **Figure 10 (a)** plots the contamination rate per unit dose for each bandwidth in the photon-limited regime. The rates are normalized to those measured for the in-band configuration of BL8 with a Be filter. The dramatic increase in contamination rate with wavelength from 10 nm to 60 nm suggests that even low intensity out-of-band radiation could pose a contamination risk to lithographic systems.

The general trend of increasing contamination rate with wavelength in the range 10 nm to 80 nm has been observed experimentally⁵³ and predicted by models.¹⁶ A likely explanation of this behavior is that both the (gas phase) photoabsorption cross section and the secondary electron yield for C increase to a maximum around 70 nm and drop rapidly at shorter wavelengths down to the C 1s absorption edge at 4.4 nm.

It should be noted that the samples exposed on BL8 were TiO₂-capped multilayers while those on BL1b were Ru-capped; however, the rates were very similar for both capping materials in all cases where growth rates have been measured on both substrates.

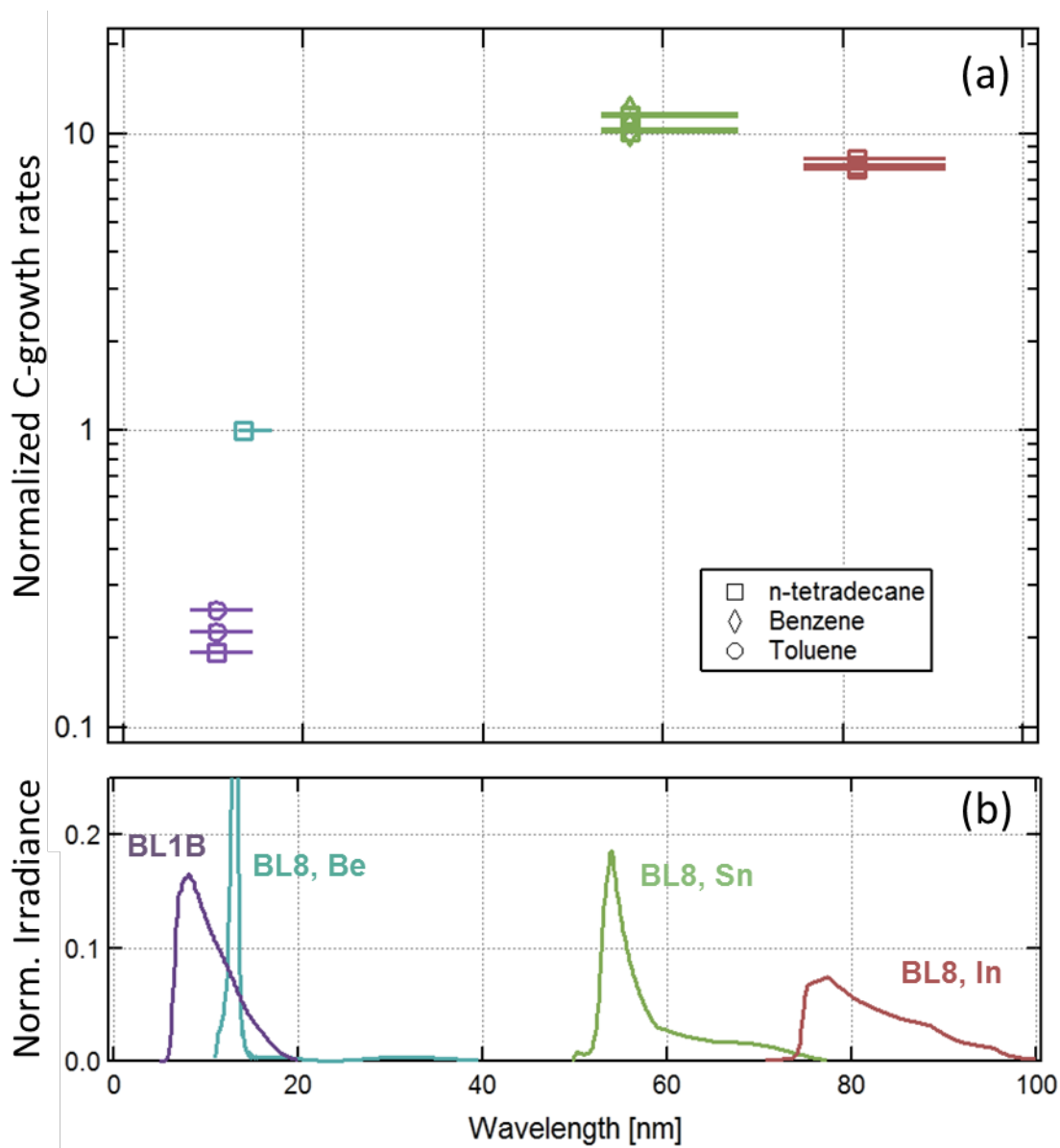


Figure 10 (a) Carbon growth rate for several wavelength bands. Horizontal bars contain 80% of power for each configuration. (b) Calculated exposure spectra for the two NIST beamlines, BL1b and BL8, shown schematically in Fig. 6. A Zr filter was used on BL1b while Be, Sn and In filters were used on BL8, as indicated. The plotted irradiance of each configuration was normalized to the area (total power) of the in-band spectra for BL8 with a Be filter.

6A.3.2.4 Metrology of EUV-induced carbon contamination

The thickness of the carbon (or oxide) deposited during contamination experiments like those discussed above was typically measured using x-ray photoelectron spectroscopy (XPS) and/or spectroscopic ellipsometry (SE). The latter technique has many practical advantages over the former. SE is more widely available than XPS, it can be performed in air rather than vacuum, and it can typically measure small contamination spots with higher spatial resolution in much less time than XPS. SE also has accuracy below a nanometer and even better repeatability when used to

measure films of known composition and optical properties (e.g., SiO₂ or films deposited by a well-characterized industrial process). Unfortunately, the structure, morphology and resulting optical properties of the carbon deposited by EUV cracking are not well known and may vary significantly depending upon the exposure conditions (as we will demonstrate below). Although it is possible to fit a reasonable optical model to a uniform, relatively thick ($\gg 10$ nm) carbonaceous film of unknown structure and simultaneously determine its thickness using SE, this procedure is not reliable for a typical EUV-contamination deposit with a distribution of thicknesses < 3 nm. Instead, a fixed optical model must be applied, even though the structure may vary across the deposit.

Since the absolute thickness determined by SE depends critically on the optical model used to fit the data, XPS is a more reliable method for comparing carbon thicknesses deposited under varying conditions. The most common method for determining thickness using XPS is to measure the attenuation of the substrate signal (e.g. the Ru 3d or 3p peaks for Ru-capped MLMs or the Ti 2p peak for TiO₂-capped MLMs) caused by the overlayer of C. To use this technique, one must assume a practical effective attenuation length (EAL) for the photoelectrons originating in the substrate as they pass through the carbon film. The resulting C thickness will be proportional to the assumed EAL. There is a range of calculated and measured EALs reported in the literature,⁴⁷ and the results presented here use 2.08 nm for Ti 2p and Ru 3p substrates as measured by Lesiak et al. for graphite with density 2.2 g/cm³. [ref. 54]

Although there is not a universally accepted value for the EAL of EUV-deposited C, this quantity is much less sensitive to variations in the morphology and composition of the carbon than the optical properties and hence thicknesses reported by SE. As reported by Hill, et al., **Figure 11** demonstrates this difference by overlaying a collection of thickness profiles from XPS and SE maps of several EUV-induced carbon deposition spots.⁴⁷ Also shown are the EUV dose profiles used to make the deposited carbon. The exposures were made at a variety of pressures, thus there is not a common correlation between dose and thickness for all the profiles. The measurements show that there is a dose-dependent discrepancy between thicknesses determined by XPS and SE that becomes quite pronounced for exposures with the largest peak doses in the center of the spots. In all cases, however, there is a good agreement in the wings of the C distributions where the local dose decreases to zero. One possible explanation of this dose-dependent correlation between XPS and SE is that the composition of the carbonaceous contamination is altered by subsequent EUV irradiation after its initial deposition. This hypothesis is supported by two previous studies. Matsunara⁵⁵ reported that irradiation of amorphous chemical-vapor-deposited C by broadband synchrotron radiation resulted in a monotonic decrease of H content and increase in density with radiation dose. Anazawa⁵⁶ examined EUV-deposited C with several different metrologies, which showed that the H content of EUV-deposited films was significantly lower in the deepest layers of the deposit that received the highest EUV dose. Both of these independent studies suggest that EUV irradiation will reduce the H content and increase the density of EUV-induced C deposits. These variations in composition will skew the thickness reported by SE since a fixed optical model must be assumed across the entire spot. These findings are consistent with the NIST results shown in Fig. 11.

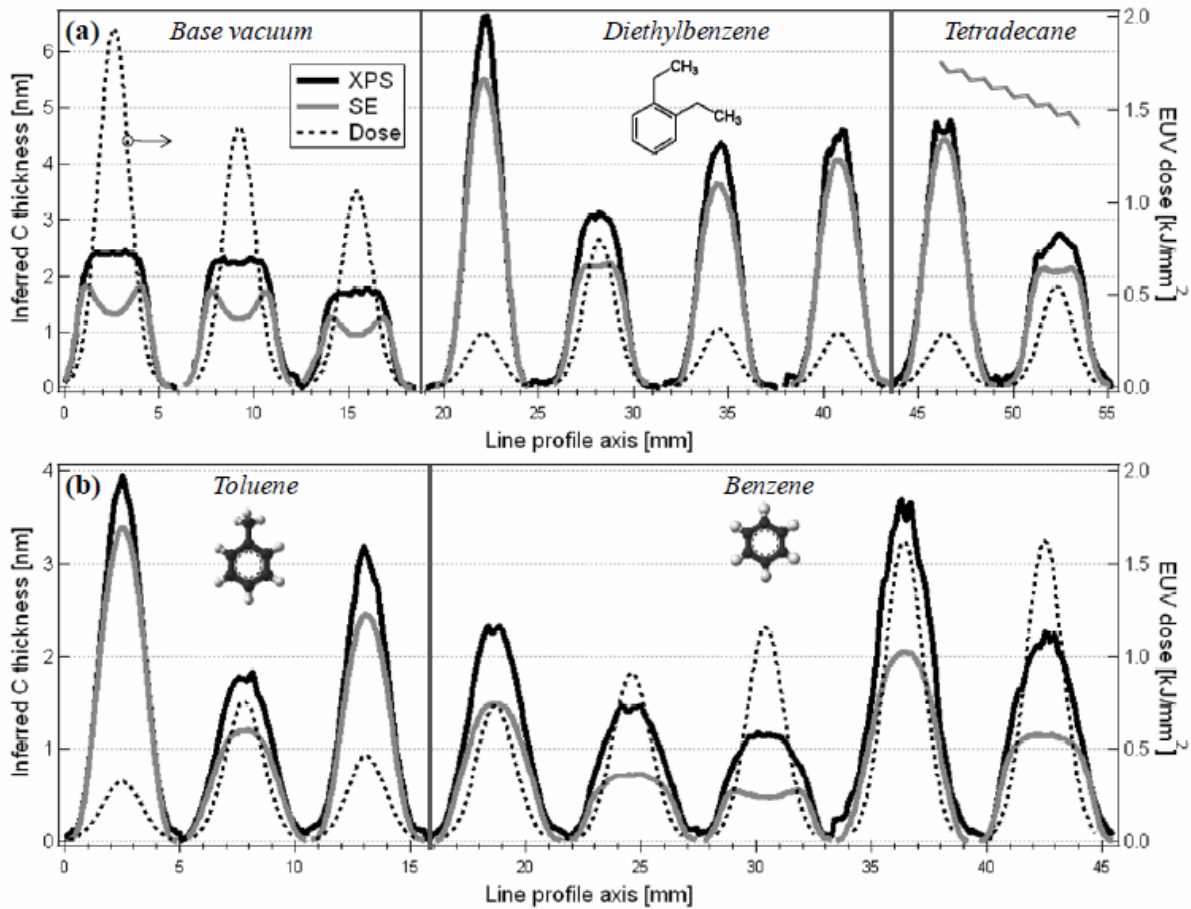


Figure 11. Collected profiles of C thickness inferred from x-ray photoelectron spectroscopy (XPS) and spectroscopic ellipsometry (SE) along lines through the centers of contamination spots created by EUV exposure exposures in (a) the base vacuum and various partial pressures of admitted diethylbenzene, tetradecane and (b) toluene and benzene. The EUV dose distributions across the exposure spots are also plotted (dashed lines, right axis).

6A.4. Resist outgas testing

6A.4.1 Early measurements

If sufficient care is taken in constructing a tool, the most probable cause of optics contamination would be the outgassing of the photoresist during EUV exposure. In order to gauge the contamination potential of this outgassing, a method was sought to qualify the photoresist before its use. Many groups worked on this problem, with three techniques used initially.

The simplest method developed was to measure outgassing by a pressure rise method.⁵⁷ This method involves measuring the pressure rise while illuminating a wafer with EUV. Using a calibrated gauge and knowing the pumping speed, the rate and total outgassing can be calculated. These tools have often been equipped with residual gas analyzers (RGAs) for partial chemical analysis. This method has the advantage of being reasonably simple, but little is learned about the

actual complicated molecular components of the outgassing because of the difficulty in interpreting the RGA spectra.

A second method employed an RGA pointed directly at the illuminated spot.^{58,59} Knowing the intercepted solid angle of the RGA and its absolute efficiency for detecting different molecules, the partial pressure and thus outgassing rate can be calculated for the different molecular fragments. Among the disadvantages is again the limited capability to interpret the RGA spectra. Additional complexities include fragmentation patterns that may be tool-specific and differences in conduction speeds among fragments of different mass. Careful calibration of each RGA over a wide mass range would also be required to compare results from different instruments.

A third method involved exposing the resist in an initially evacuated, unpumped chamber. After the exposure is complete, the chamber is filled with helium, which flows through the chamber and through a thermal desorption tube.^{60,61} Organics stick to the desorption medium. The tube is subsequently removed from the chamber and analyzed by a gas chromatograph with a mass spectrometer detector (GC/MS). Helium is again flowed through the tube while it is heated, and the organics become volatilized and are subsequently deposited into a small cold region at the head of the GC column (cryofocus). Releasing the sample into the chromatography column separates species depending on their mobility, thus enabling a more specific analysis of the mass spectra than the RGA method, in which all outgas products (as well as background gases) are present all the time. However, the desorption tubes have sticking coefficients that are less than unity and vary with species and thus skew the chemical analysis.

SEMATECH conducted a round-robin with eight labs employing the three techniques described above.⁴³ The results for total outgassing differed by four orders of magnitude among the labs; however if the highest and lowest results are not used, the results were within a factor of 30. The labs using the desorption-tube method had the two lowest results, but there was no pattern among the labs using the total pressure rise method and the RGA method.

The large disparities observed in the SEMATECH round-robin motivated the development of a fourth method with less uncertainty. This method combined the total pressure rise with a subsequent chemical analysis.⁶² Before the EUV was turned on, all pumping of a very small chamber was valved off and the pressure rate-of-rise was measured with a calibrated gauge. The pressure rise was monitored during and after EUV illumination, and the difference between the final pressure and that expected based on the background outgassing was the total rise due to the photoresist outgassing during illumination. The outgas products were then collected by cooling a trap to liquid-nitrogen temperature, and these were subsequently analyzed in a GC/MS with cryofocus. The trap collected all outgas products heavier than CO. Also, the very small volume of the chamber led to significant pressure rises that were easily measured by a calibrated capacitance-diaphragm gauge, which is species-independent. However, the heaviest, least-volatile outgas products likely deposited onto the chamber walls and were thus not counted in the pressure-rise nor trapped in the cryotrap.

In a subsequent intercomparison among three of the eight labs involved in the round-robin, NIST, imec, and CNSE, found agreement within 30% for the total outgassing and identification of the same species.⁶³

Contemporaneous with the photoresist outgas testing activity was a measurement to determine the relative contributions of the outgassing from photoresist and from the tool itself. The measurement, which was a modified version of the fourth outgassing method, was employed on one of the first pre-production microexposure tools at Intel.⁶⁴ In this case a large liquid nitrogen cooled trap was employed and opened to the tool for several hours. Subsequent GC/MS analysis of the collected material found ketones and aldehydes, likely from partial oxidation of hydrocarbon contaminants, as well as silicones, likely introduced from the ambient air in the clean room either during servicing or during the use of the loadlock. Subsequent EUVL tools were constructed and maintained with more attention to cleanliness and did not suffer from these sorts of contamination.

6A.4.2 Witness-sample testing

The intercomparison difficulties described above caused ASML and others in the EUVL community to conclude that not only were there difficulties in the standardization of intercomparisons, but there also was not a reliable method to predict the optics contamination from the available measurements, including chemical analyses of the photoresist outgas. For this reason ASML proposed witness-sample testing in 2006. (See ref. ⁶⁵)

The witness-sample test consists of irradiating a witness sample in the same vacuum environment as a simultaneously irradiated photoresist. The thickness of the carbon contamination on the witness sample produced by the resist outgassing was subsequently measured using spectroscopic ellipsometry with an optical model specified by ASML. The carbon was then removed with hot-filament-generated atomic hydrogen, and the witness sample was analyzed using XPS to check for non-cleanable trace elements. During the exposure portion of the test, the dose to the resist must be the dose-to-clear (E_0) as measured on that tool, and the witness sample must have a Ru surface so that its behavior mimics that of a Ru-capped multilayer. The illumination of the resist and witness sample may be EUV photons or electrons, but the irradiation of the witness sample must have sufficient intensity or current to lead to mass-limited growth. With mass-limited growth, test depends more on the characteristics of the resist than of the exposure tool

Witness-sample testing is time-consuming and expensive, so many attempts have been made to develop alternate tests through simpler means. Many of the witness-sample-testing tools are fitted with RGAs capable of measuring low outgassing levels, and the resulting RGA spectra obtained during exposure can be correlated with the results of contamination-growth tests. Pollentier et al.⁶⁶ found that the contamination growth correlates well with an integral over the mass spectrum, where the integrand is the product of the RGA signal with the mass raised to an empirically determined power. This correlation is likely due to the availability of an increasing number of carbon atoms, plus the lower volatility of species with greater masses. Unfortunately, the correlation, while useful, is not well understood because it appears to depend on whether the exposure was performed by EUV or electrons and it varies with electron-beam energy.

Another correlation effort at the Evolving nano-process Infrastructure Development Center (EIDEC) focused on the grouping of resists into families whose composition (polymer backbone, photo-acid generator (PAG) and quencher loading) was identical.⁶⁷ This study found that if the resist components are the same, the contamination growth increases with both PAG and quencher

loading. Thus, the maximum contamination growth from this resist family would be that from a formulation that has the highest expected PAG and quencher loading. A similar study found that the higher loading led to a greater contamination at the same dose, but that E_0 of the resist can be reduced enough that the contamination growth at E_0 is actually lower.⁶⁸ Later work at SEMATECH investigated different resist families with known PAG concentrations. When the concentrations of protecting unit and quencher were fixed, the carbon growth was correlated linearly with value of E_0 , with the resist having the largest PAG concentration being the least contaminating.⁶⁹

ASML's original specification for the witness-sample test required, for the exposure of one 300 mm wafer equivalent, less than 3 nm of contamination growth on the witness sample and, after hydrogen cleaning, less than a 0.23 % reflectivity decrease caused by non-cleanable contamination (0.16 % for second-generation tools).⁷⁰ In 2014, the unexpectedly good performance of in-tool mitigation³ allowed the contamination growth to be relaxed to 10 nm⁷¹, and in February 2015 the test requirement of all conventional chemically amplified resists was suspended for the rest of the year.⁷² The suspension was made permanent later that year at the IEUVI Resist TWG at the EUVL Symposium (27-29 October 2014, Washington, DC). During 2011-2015, the witness-sample test was key to the EUVL industry's cautious approach in avoiding contamination from photoresist outgassing. That caution provided a margin of safety that allowed users to gain experience with preproduction scanners and demonstrate the effectiveness of hydrogen-based in-tool mitigation techniques.

6A.4.3 Witness-sample testing; non-conventional resists

The requirements for resist outgas testing were re-examined with the advent of novel resists such as nanoparticle-containing hybrids,⁷³ metal-oxide-based resists,⁷⁴ and organometallic resists.⁷⁵ Previous outgassing studies were performed entirely on organic materials with a limited number of constituent elements, so the presence of outgas containing metallic elements such as Sn, Hf, Bi, etc., in a hydrogen atmosphere creates new concerns about the cleanability of various reaction products. The outgassing of some of these resists has been measured and found to be low, but until recently, this was done with a standard witness-sample test, which happens in a vacuum without the presence of hydrogen. Since the atmosphere in an EUVL scanner may contain as much as 1 mbar hydrogen,^{76,77,78} and many metals form hydrides or other hydrogen-containing compounds which may not be cleanable, ASML promoted the development of testing in a hydrogen atmosphere that mimics the scanner environment in which the pulsed EUV is intense enough to generate hydrogen radicals.⁷⁹

EIDEC responded to ASML's need by developing the High Power EUV Irradiation Tool⁸⁰ which has used a witness sample test to qualify the non-conventional resists since Q3 in 2015. The tool was also used to demonstrate that the irradiation of a model material, such as SnO₂, in a hydrogen atmosphere can create a non-cleanable deposit on a Ru-capped witness sample. The need for such qualification tests in the future is however uncertain since ASML announced its intention to install a membrane in the dynamic gas lock to prevent any resist outgas from getting to any of the optics.⁸¹ Even though meeting a certain set of criteria may no longer be a necessary condition for the use of a given resist, some measure of the outgas characteristics of a resist may

still be used in its evaluation since the long term effect in HVM of various outgas products on the dynamic gas lock membrane and other parts of the wafer chamber are still unknown.

6A.5 Cleaning and contamination-control

Carbon deposition on surfaces can be of several different forms. The EUV-deposited carbon on the projection optics in a hydrogenated, polymeric version⁸² while that deposited in the environment of the source has a predominant diamond-like nature,⁸³ with the former version having a much faster cleaning rate than the latter.^{83, 84} Activated oxygen, such as ozone or atomic oxygen, has been commonly used to clean synchrotron optics and was demonstrated as effective at removing of EUV-deposited carbon from a TiO₂-capped multilayer.⁸⁵ If overused, however, these gases can irreversibly oxidize the optical surface, especially a non-oxide cap layer material such as ruthenium. Nishiyama et al. have achieved some success in reversing oxidation in ruthenium-capped multilayers with atomic-hydrogen,⁸⁶ but there is concern that repeated cleanings using activated oxygen might create a stoichiometric version that cannot be reversed. Atomic hydrogen for stand-alone systems can be created efficiently using a hot filament⁸⁷ and such a system was used to demonstrate efficient and non-damaging removal of EUV-deposited polymeric carbon.⁸⁸

Controlling contamination in an actual tool is a three-pronged strategy. First, measures are taken to reduce the transport of the resist outgas from the wafer to the optical surfaces; second, a mitigating gas which can provide real time cleaning action is introduced; and third, periodic in situ or ex situ cleaning cycles may be provided. A significant advance of the first prong was described in 2000 by Mertens et al.⁸⁹: a dynamic gas lock that reduced the conductance of heavy organics by five orders of magnitude while reducing EUV transmission by only 5 %. More recently, ASML has advanced this approach as reported in its patents for gas locks and curtains.^{76 - 78} The atmosphere within the scanner is proprietary, but it most likely includes hydrogen as a mitigating gas, whose interaction with high-intensity EUV radiation produces atomic and ionic hydrogen. ASML and its collaborating laboratories have studied this phenomenon⁹⁰ and its capability to remove carbon.² Finally, research in generating plasmas for both in situ and ex situ cleaning operations is being conducted by ASML and its collaborating laboratories^{2, 91} in the event that the real time mitigation is inadequate.

6.A.6 Summary and future outlook

The study of optics contamination was a critical component of the research and development effort for EUVL from the very beginning of that enterprise. Through the work of several laboratories worldwide, the two major mechanisms for degradation of the projection optics, EUV-induced oxidation and carbonization, were better understood and brought under control. Degradation of the optics by oxidation in the tool environment was reduced to a negligible level by the use of a 2 nm cap layer of Ru. Carbonization was eliminated as a problem by the use of hydrogen both to form gas curtains that limited the exposure of the optics to the outgassing from resists and other organic materials in the tool and most likely to provide hydrogen radicals that inhibited carbon deposition during operation. Atomic hydrogen can also be used in cleaning cycles to remove any accumulated carbon deposits resulting from extended operation.

A new generation of metal-containing resists are showing promise for very high resolution patterning. There is now concern that some metal ions can be liberated by hydrogen which may not be cleaned from optical surfaces once they've been deposited. More study of this emerging field is necessary.

Attention has now turned to providing contamination mitigation and cleaning to the condenser optics which are exposed to the debris from a very hot tin (Sn) plasma. Here the degradation is caused by the deposition of Sn and the possible sputtering due to the fast ions.⁹² Hydrogen radicals are also effective for removing Sn since they form SnH₄ which is volatile at the operating temperature of the optics.⁹³ However, redeposition due to the decomposition of SnH₄ and possible benefits from cap layers different from Ru are still issues under study.⁹⁴

6.A.7 References

- ¹ H. Oizumi, et al., "Contamination Removal from EUV Multilayer Using Atomic Hydrogen Generated from Heated Catalyzer," *Proc. SPIE* 5751, 1147 - 1154 (2005).
- ² A. Dolgov, et al., "Comparison of H₂ and He carbon cleaning mechanisms in extreme ultraviolet-induced and surface wave discharge plasmas," *J. Phys. D: Appl. Phys.* **47** (2014).
- ³ U.S. Patent No. 8,625,068 B2 Nienhysw et al. assigned to ASML.
- ⁴ D. Berthelot and H. Gaudenchon, "The chemical effects of ultraviolet rays on gaseous bodies -- the effects of polymerisation," *Comptes Rendus Hebdomadaires des Seances de l'Academie des Sciences* 150, 1169-1172 (1910).
- ⁵ R. Lariviere Stewart, "Insulating films formed under electron and ion bombardment," *Phys. Rev.* 45, 488-490 (1934).
- ⁶ J. H. L. Watson, "An effect of electron bombardment upon carbon black," *J. Appl. Phys.* 18, 153-161 (1947).
- ⁷ J. Hillier, "On the investigation of specimen contamination in the electron microscope," *J. Appl. Phys.* 19, 226 (1948).
- ⁸ K. Boller, R. P. Haelbich, H. Hogrefe, W. Jerk, and C. Kunz, "Investigation of carbon contamination of mirror surfaces exposed to synchrotron radiation," *Nucl. Instrum. Method.* **208**, 273-279 (1983).
- ⁹ V. Domingo, B. Fleck, and A. Poland, "The SOHO mission: An overview," *Solar Phys.* 162, 1-37 (1995).
- ¹⁰ A. BenMoussa et al., "On-orbit degradation of solar instruments," *Solar Phys.* 288, 389-434 (2013).
- ¹¹ E. Spiller, "Low-loss reflectivity coatings using absorbing materials," *Appl. Phys. Lett.* 20, 365-367 (1972).
- ¹² T. W. Barbee Jr., J. C. Rife, W. R. Hunter, M. P. Kowalski, R. G. Cruddace, and J. F. Seely, "Long-term stability of a Mo/Si multilayer structure," *Appl. Opt.* **32**, 4852-4854 (1993).
- ¹³ J. H. Underwood, E. M. Gullikson, and K. Nguyen, "Tarnishing of Mo/Si multilayer mirrors," *Appl. Opt.* 32, 6985-6990 (1993).
- ¹⁴ D. Gaines, R. C. Spitzer, N. M. Ceglio, M. Krurey, and G. Ulm, "Radiation hardness of molybdenum silicon multilayers designed for use in a soft x-ray projection lithography system," *Appl. Opt.* **32**, 6991-6998 (1993).
- ¹⁵ M. Wedowski, S. Bajt, J. A. Folta, E. M. Gullikson, U. Kleinberg, L. E. Klebanoff, M. E. Malinowski, and W. M. Clift, "Lifetime studies of Mo/Si and Mo/Be multilayer coatings for extreme ultraviolet lithography," *Proc. SPIE* **3767**, 217-224 (1999).
- ¹⁶ J. Hollenshead and L. Klebanoff, "Modeling radiation-induced carbon contamination of extreme ultraviolet optics," *J. Vac. Sci. Technol.* B24 (2006) 64-82.

-
- ¹⁷ J. Hollenshead and L. Klebanoff, "Modeling extreme ultraviolet/H₂O oxidation of ruthenium optic coatings", *J. Vac. Sci. Technol.* B24 (2006) 118-130.
- ¹⁸ A. F. G. Leonowich and A. P. Hitchcock, "Secondary electron deposition mechanism of carbon contamination," *J. Vac. Sci. Tech* B30, 030601 (2012).
- ¹⁹ A. F. G. Leontowich, A. P. Hitchcock, "Secondary electron deposition mechanism of carbon contamination," presented at 11th International Conference on Synchrotron Radiation Instrumentation, Saint-Aubin, France, 16 July, 2012.
- ²⁰ S. Bajt, J. B. Alameda, T. W. Barbee, Jr, W. M. Clift, J. A. Folta, B. Kaufmann, and E. A. Spiller, "Improved reflectance and stability of Mo-Si multilayers," *Opt. Eng.* 41, 1797-1804 (2002).
- ²¹ S. Bajt, N.V. Edwards, and T. E. Madey, "Properties of ultrathin films appropriate for optics capping layers exposed to high energy photon irradiation," *Surf. Sci. Rep.* **63**, 73–99 (2008).
- ²² D. L. Windt, "IMD: Software for modeling the optical properties of multilayer films," *Computer in Physics* **12**, 360–371 (1998).
- ²³ http://www-cxro.lbl.gov/optical_constants/ web page, maintained by E. M. Gullikson.
- ²⁴ S. Bajt, H. N. Chapman, N. Nguyen, J. Alameda, J. C. Robinson, M. Malinowski, E. Gullikson, A. Aquila, C. Tarrío, and S. Grantham, "Design and performance of capping layers for extreme-ultraviolet multilayer mirrors," *Appl. Opt.* **42**, 5750–5758 (2003).
- ²⁵ S. Bajt, et al., "Lifetime Benchmarking of EUV Multilayer Optics: Report on Screening Tests of Multilayer 2," Project Report for LITH160, 2004.
- ²⁶ K. Ro, W. Park, G. Choe, J. Ahn, *Korean J. Mater. Res.* **7**, 21 (1997).
- ²⁷ S.-H. Kim et al., "Influence of sputtering parameters on microstructure and morphology of TiO₂ thin films", *Mat. Lett.* **57**, 343 (2002).
- ²⁸ S. Bajt, S. Hau-Riege, Z. R. Dai, J. Alameda, E. Nelson, C. Evans, J. S. Taylor, F. Dollar, S. Hill, M. Chandhok, M. Fang, "Protective capping layer for EUVL optics using TiO₂" EUVL Symposium, San Diego, USA, 2005.
- ²⁹ S. Yulin, N. Benoit, T. Feigl, N. Kaiser, M. Fang, and M. Chandhok, "Mo/Si multilayers with enhanced TiO₂ and RuO₂ capping layers," *Proc. SPIE* 6921, 692118 (2008).
- ³⁰ M. Kriese, Yu. Platonov, J. Rodriguez, G. Fournier, S. Grantham, C. Tarrío, J. Curry, S. B. Hill, and T. B. Lucatorto, "Development and evaluation of interface-stabilized and reactive-sputtered oxide-capped multilayers for EUV lithography," *Proc. SPIE* Vol. 9422, 9422-19 (2015).
- ³¹ M. Malinowski, P. Grunow, C. Steinhaus, M. Clift, and L. Klebanoff, "Use of molecular oxygen to reduce EUV-induced carbon contamination of optics," *Proc. SPIE* **4343**, 347–356 (2001).
- ³² M. E. Malinowski, C. A. Steinhaus, D. E. Meeker, W. M. Clift, L. E. Klebanoff, and S. Bajt, "Relation between electron- and photon-caused oxidation in EUVL optics," *Proc. SPIE* **5037** 429–438 (2003).
- ³³ Y. Kakutani, M. Niibe, K. Kakiuchi, H. Takase, S. Terashima, H. Kondo, S. Matsunari, T. Aoki, Y. Gomei, and Y. Fukuda, "A reflectance measurement system for investigating radiation damage to EUVL mirrors in New-SUBARU," *Proc. SPIE* **5533**, 47–57 (2004).
- ³⁴ M. Weiss, M. Wedowski, H. Trenkler, B. Mertens, B. Wolschrijn, R. Jansen, A. vd Runstraat, K. Spee, R. Klein, S. Ploger, E. Louis, R. vd Kruijs, R. Kurt, H. Meiling, and R. Moors, "The optics contamination/lifetime program: an overview of supporting facilities," presented at The Second International EUVL Symposium, Septemebr 30 – October 2, 2003, Antwerp, Belgium.
- ³⁵ R. Klein, A. Gottwald, F. Scholze, R. Thornagel, J. Tümmler, G. Ulm, M. Wedowski, F. Stietz, B. Mertens, N. Koster, and J. van Elp, "Lifetime testing of EUV optics using intense synchrotron radiation at the PTB radiometry laboratory," *Proc. SPIE* **4506**, 105–112 (2001).
- ³⁶ S. Oestreich, R. Klein, F. Scholze, J. Jonkers, E. Louis, A. Yakshin, P. Gorts, G. Ulm, M. Haidl, and F. Bijkerk, "Multilayer reflectance during exposure to EUV radiation," *Proc. SPIE* **4146**, 64 (2000).
- ³⁷ N. Koster, B. mertens, R. Jansen, A. vdRunstraat, F. Stietz, M. Wedowski, H. Meiling, R. Klein, A. Gottwald, F. Scholze, M. Visser, R. Kurt, P. Zalm, E. Louis, and A. Yakshin, "Molecular contamination mitigation in EUVL by environmental control," *Microelectronic Engineering* **61–62**, 65 (2002).

-
- ³⁸ C. Tarrío and S. Grantham, "Synchrotron beamline for extreme-ultraviolet multilayer mirror endurance testing," *Rev. Sci. Instrum.* **76**, 056101-1 (2005).
- ³⁹ C. Tarrío, S. Grantham, S. B. Hill, N. S. Faradzhev, L. J. Richter, and T. B. Lucatorto, "A synchrotron beamline for extreme-ultraviolet photoresist testing," *Rev. Sci. Instrum.* **82**, 073102 (2011).
- ⁴⁰ Y. Gomei, Y. Kakutani, H. Takase, M. Niibe, S. Terashima, T. Aoki, and S. Matsunari, "The role of ambient hydrocarbon species to reduce oxidation in Ru capping layers for EUVL optics mirrors," *Microelectron. Eng.* **83**, 676–679 (2006).
- ⁴¹ S. B. Hill, I. Ermanoski, S. Grantham, C. Tarrío, T. B. Lucatorto, T. E. Madey, S. Bajt, M. Chandhok, P. Yan, O. Wood, S. Wurm, and N. V. Edwards, "EUV testing of multilayer mirrors: critical issues," *Proc. SPIE* **6151**, 61510F-1 (2006).
- ⁴² T. E. Madey, N. S. Faradzhev, B. Y. Yakshinskiy, and N. V. Edwards, "Surface phenomena related to mirror degradation in extreme ultraviolet (EUV) lithography," *Appl. Surf. Sci.* **253**, 1691–1708 (2006).
- ⁴³ K. R. Dean et al., "An analysis of EUV resist outgassing measurements," *Proc. SPIE* 6519, 65191P (2007).
- ⁴⁴ C. Tarrío, R. E. Vest, T. B. Lucatorto, and R. Caudillo, "Tracking down sources of carbon contamination in EUVL exposure tools," *Proc. SPIE* 7271, 727112 (2009).
- ⁴⁵ Bas Wolschijn, Rik Jansen, Arnold Storm, Roland van Vliet, Bas Mertens, Dirk Ehm, Marco Wedoski, Thomas Stein, Roel Moors, and Vadim Banine, "Progress in optics lifetime program for ASML for EUV lithographic tools," presented at the EUVL Symposium, San Diego November 7 – 9, 2005.
- ⁴⁶ S. B. Hill, N. S. Faradzhev, C. Tarrío, T. B. Lucatorto, R. A. Bartynski, B. Yakshinskiy, and T. E. Madey, "Measuring the EUV-induced contamination rates of TiO₂-capped multilayer optics by anticipated production-environment hydrocarbons," *Proc. SPIE* **7271**, 727113 (2009).
- ⁴⁷ S. B. Hill, N. S. Faradzhev, L. J. Richter, S. Grantham, C. Tarrío, T. B. Lucatorto, S. Yulin, M. Schürmann, V. Nesterenko, T. Feigl, "Optics contamination studies in support of high-throughput EUV lithography tools." *Proc. SPIE* 7969, 79690M-1 (2011).
- ⁴⁸ B. V. Yakshinskiy, "Carbon film growth on model electron-irradiated MLM cap layer: interaction of benzene and MMA vapor with TiO₂ surface," *Proc. SPIE* Vol. **7271**, 727110 (2009).
- ⁴⁹ S. Zalkind, B. V. Yakshinskiy, and T. E. Madey, "Interaction of benzene with TiO₂ surfaces: Relevance to contamination of extreme ultraviolet lithography mirror capping layers," *J. Vac. Sci. Technol. B* **26**, p. 2241 (2008).
- ⁵⁰ M. I. Temkin and V. Pyzhov, "Recent modifications to Langmuir isotherms," *Acta Physicochimica U.R.S.S.* **12**, p. 217-222 (1940)
- ⁵¹ I. Langmuir, "The adsorption of gases on plane surfaces of glass, mica, and platinum," *J. Am. Chem. Sci.* **40**, 1361-1403 (1918).
- ⁵² S. B. Hill, N. S. Faradzhev, L. J. Richter, and T. B. Lucatorto, "Complex species and pressure dependence of intensity scaling laws for contamination rates of EUV optics determined by XPS and ellipsometry," *Proc. SPIE* 7636, 76360E (2010).
- ⁵³ P. Thomas et al., "Wavelength dependence of carbon contamination on mirrors with different capping layers," *Proc. SPIE* **7636**, 76361X (2010).
- ⁵⁴ Lesiak B., Jablonski A., Prussak Z., Mrozek P. "Experimental determination of the inelastic mean free path of electrons in solids" *Surf. Sci.* **223**, p. 213-232 (1989).
- ⁵⁵ T. Matsuura, S. Okubo, K. Oda and T. Ushiro, "Development of Refractive-Index Modulated Diffractive Optical Element Using a-C:H Film," *SEI Technical Review* **65**, p. 31 (2007)
- ⁵⁶ T. Anazawa, et al, "Cleaning of carbon contamination on EUV masks and optics," *Proc. SPIE*, 7969-22 (2011)
- ⁵⁷ S. Kobayashi, J. J. Santillan, H. Oizumi, and T. Itani, "EUV resist outgassing quantification and application," *Proc SPIE* 7273, 72731P (2009).
- ⁵⁸ H. Hada, T. Watanabe, K. Hamamoto, H. Kinoshita, and H. Komano, "Evaluation of resists outgassing by EUV radiation," *Proc. SPIE* 5374, 686-694 (2004).
- ⁵⁹ G. Denbeaux et al., "Quantitative measurement of EUV resist outgassing," *Proc. SPIE* 6533, 653318

(2007).

⁶⁰ W. Yueh, H. B. Cao, V. Thirumala, and H. Choi, "Quantification of EUV Resist Outgassing," Proc. SPIE 5753, 765-770 (2005).

⁶¹ K. R. Dean, K. E. Gonsalves, and M. Thiagarajan, "Effects of material design on EUV resist outgassing," Proc. SPIE 6153, 61531E (2006).

⁶² C. Tarrío, "Method for the characterization of extreme-ultraviolet photoresist outgassing," J. Res. NIST 114, 179-183 (2009).

⁶³ C. Tarrío, I. Pollentier, C. Mbanaso, G. Denbeaux, and A. Antohe, "Summary of OS1 outgassing results by NIST, IMEC, and CNSE", presented at EUVI Resist TWG, (2009).

⁶⁴ C. Tarrío, R. E. Vest, T. B. Lucatorto, and R. Caudillo, "Tracking down sources of carbon contamination in EUVL exposure tools," Proc. SPIE 7271, *Alternative Lithographic Technologies*, 727112 (2009).

⁶⁵ B. Wolschrijn, R. Moors, and D. Elm, "New method for resist outgassing qualification," IEUVI Resist TWG, Barcelona, Spain, 20 October, 2006.

⁶⁶ I. Pollentier, R. Lokasani, R. Gronheid, S. Hill, C. Tarrío, and T. Lucatorto, "Relationship between resist-related outgassing and witness-sample contamination in the NXE outgas qualification using electrons and photons," Proc. SPIE 8679, 8679K (2013).

⁶⁷ I. Takagi et al., "Comparison of resist family outgassing characterization between EUV and EB," J. Photopolymer Sci. Tech. 26, 673-678 (2013).

⁶⁸ S-H. Chang et al., "Balancing lithographic performance and resist outgassing in EUV resists," Proc. SPIE 8679, 867900 (2013).

⁶⁹ Y-J. Fan, K. Maruyama, R. Ayothi, T. Naruoka, T. Chakraborty, D. Ashworth, J.S. Chun, C. Montgomery, S-H. Jen, M. Neisser, K. Cummings, "First results of outgas resist family test and correlation between outgas specifications and EUV resist development", Proc. SPIE 9422, 942211 (2015).

⁷⁰ N. Harned, "NXE resist outgas testing update," IEUVI Resist TWG, Miami, FL, 20 October, 2011.

⁷¹ N. Harned, "ASML Update," IEUVI Resist TWG, San Jose, CA, 23 February, 2014.

⁷² N. Harned, "Resist outgassing spec relaxation," IEUVI Resist TWG, San Jose, CA, 22 February, 2015.

⁷³ L. Li, S. Chakrabarty, K. Spyrou, C. K. Ober, and E. P. Giannelis, "Studying the mechanism of hybrid nanoparticle photoresists: Effect of particle size on photopatterning," Chemistry of Materials 27, 5027-5031 (2015).

⁷⁴ A. Grenville et al., "Integrated fab process for metal oxide EUV photoresist," Proc. SPIE 9425, 94250S (2015).

⁷⁵ J. Passarelli et al., "Organometallic carboxylate resists for extreme ultraviolet with high sensitivity," J. Micro-Nanolith., MEMS, and MOEMS 14 043503 (2015).

⁷⁶ D.H. Ehm, J.H.J. Moors, B.T. Wolschrijn, V. Banine, V.V. Ivanov, "Method for removing contamination of optical surfaces and optical arrangement", US patent 8,279,397 B2 (2012).

⁷⁷ D.H. Ehm, J.H.J. Moors, B.T. Wolschrijn, T. Stein, E. te Slighte, "Method for removing a contamination layer from an optical surfaces and arrangement therefor as well as a method for generating a cleaning gas and arrangement therefor", US patent 8,419,862 B2 (2013).

⁷⁸ H-K. Nienhuys, P.G. Jonkers, A.M.A. Huijberts, "Lithographic apparatus configured to suppress contamination from passing into the projection system and method", US patent 8,625,068 B2 (2014).

⁷⁹ ASML presentation at the Resist TWG, San Jose, CA, February 2015.

⁸⁰ E. Shiobara, S. Mikami, and S. Tanaka, "The Recent Study of Resist Outgassing in the Hydrogen Environment", EUVL Symposium, Hiroshima, Japan, October 2016.

⁸¹ Yu-Jen Fan, SEMATECH presentation at the Resist TWG, EUVL Symposium, Hiroshima Japan, October 2016.

⁸² Juequan Chen, et al., "Detection and characterization of carbon contamination on EUV multilayer mirrors," Optics Express 17, 16969 (2009).

⁸³ A. Dolgov, et al., "Characterization of carbon contamination under ion and hot atom bombardment in a tin plasma extreme ultraviolet light source," Appl. Surf. Sci. 353, 708 (2015).

-
- ⁸⁴ Juequan Chen, et al., "In situ ellipsometry study of atomic hydrogen etching of extreme ultraviolet induced carbon layers," *Appl. Surf. Sci.* **258**, 7 (2011).
- ⁸⁵ N. Faradzhev, et al. "EUV-Driven Carbonaceous Film Deposition and Its Photo-oxidation on a TiO₂ Film Surface," *J. P. Chem.* 117, 23072-23081 (2013).
- ⁸⁶ I. Nishiyama, H. Oizumi, K. Motai, A. Izumi, T. Ueno, H. Akiyama, and A. Namiki, "Reduction of oxide layer on Ru surface by atomic-hydrogen treatment", *J. Vac. Sci. Technol. B* 23, 3129-3131 (2005).
- ⁸⁷ J. T. Yates, Jr., *Experimental Innovations in Surface Science*, Springer-Verlag, New York, 1997, chapter 201.
- ⁸⁸ S. Graham, C. Steinhaus, M. Clift, L. Klebanoff, and S Bajt, "Atomic hydrogen cleaning of EUV multilayer optics," *Proc. SPIE* 5037, 460-469 (2003).
- ⁸⁹ B. Mertens et al., "Mitigation of surface contamination from resist outgassing in EUV lithography," *Microelectronic Eng.* 53, 659-662 (2000).
- ⁹⁰ R. M. van der Horst, et al., "Exploring the electron density in plasma induced by EUV radiation: I. Experimental study in hydrogen," *J. Phys. D: Appl. Phys.* **49**, 145203 (2016).
- ⁹¹ TNO presentation "New developments in cleaning of EUVL mirrors and reticles," at the EUVL Symposium Prague, October 18 – 221, 2009.
- ⁹² R. C. Wieggers, et al., "A particle-in-a-cell plus Monte Carlo study of plasma-induced damage of normal incidence collector optics used in extreme ultraviolet lithography," *Jour. Appl. Phys.* **103**, 013308 (2008).
- ⁹³ M. M. J. W. van Herpen, et al., "Sn etching with hydrogen radicals to clean EUV optics," *Chem. Phys. Lett.* **484**, 197 (2010).
- ⁹⁴ D. Ugur, et al., "Decomposition of SnH₄ molecules on metal and metal oxide surfaces," *Appl. Surf. Science* **288**, 673 (2014).